Introductory Lecture

Probing wavepacket dynamics with femtosecond energy- and angle-resolved photoelectron spectroscopy

Kazuo Takatsuka,[a] Yasuki Arasaki,[a] Kwanghsi Wang[b] and Vincent McKoy*[b]

[a] *Department of Basic Science, Graduate School of Arts and Sciences, University of Tokyo, Komaba, 153-8902, Tokyo, Japan*
[b] *Laboratory for Molecular Sciences, Division of Chemistry and Chemical Engineering, California Institute of Technology, Pasadena, California 91125, USA*

Received 6th April 2000
Published on the Web 15th June 2000

Several recent studies have demonstrated how well-suited femtosecond time-resolved photoelectron spectra are for mapping wavepacket dynamics in molecular systems. Theoretical studies of femtosecond photoelectron spectra which incorporate a robust description of the underlying photoionization dynamics should enhance the utility of such spectra as a probe of wavepackets and of the evolution of electronic structure. This should be particularly true in regions of avoided crossings where the photoionization amplitudes and electronic structure may evolve rapidly with geometry. In this paper we present the results of studies of energy- and angle-resolved femtosecond photoelectron spectra for wavepackets in the diatomic systems, Na_2 and NaI. Both cases involve motion through regions of avoided crossings. In Na_2, however, wavepacket motion occurs on a single adiabatic potential with an inner and outer well and a barrier between them, while in NaI wavepackets move on the nonadiabatically coupled covalent (NaI) and ionic (Na^+I^-) potentials. Results of these studies will be used to illustrate the insight into wavepacket dynamics that time-resolved photoelectron spectra provide. For example, in the case of NaI these angle-resolved photoelectron spectra seem to offer some promise for probing real-time dynamics of intramolecular electron transfer occurring in the crossing region of the ionic and covalent states.

Introduction

Femtosecond time-resolved spectroscopy has now been widely exploited in numerous applications ranging from fundamental studies of real-time motion in the photodissociation of NaI to studies of electron transfer.[1–3] In this spectroscopy, a femtosecond pulse (pump) is used to lauch a wavepacket onto a state where it evolves in accordance with the time scales for vibrational ($\sim 10^{-13}$ s) and rotational ($\sim 10^{-10}$ s) motion. The evolution of the wavepacket is monitored by time-delayed femtosecond excitation to a higher electronic state which serves as a template. Various techniques including absorption, laser-induced fluorescence, multiphoton ionization, photoelectron spectroscopy, time-resolved mass spectroscopy, and stimulated emission pumping have been used to probe these wavepackets.[2–8]

DOI: 10.1039/b002739l

Time-resolved ionization offers several advantages as a probe of these wavepackets.[5,9–11] For example, the ground state of an ion is often more readily characterized than higher excited states of the molecule. Ionization also provides ions and photoelectrons and while ion detection provides mass and kinetic-energy resolution, pump–probe photoelectron spectra are well suited for monitoring wavepacket dynamics and the evolution of electronic structure along all energetically allowed internuclear distances simultaneously.[5–8] This advantage of time-resolved photoelectron spectroscopy has already been well demonstrated in the picosecond domain.[12–14] Its potential for probing molecular dynamics in the femtosecond regime has also been exploited experimentally for several systems.[5–7,15] Furthermore, Davies *et al.*[8] have recently reported results of the first femtosecond photoelectron–photoion coincidence imaging studies of photodissociation dynamics.

Efforts to map vibrational wavepackets with the help of femtosecond pump–probe techniques and energy-resolved photoelectron spectra were clearly stimulated by the seminal studies of Engel, Meier and Braun[16] who showed how the dynamics of a vibrational wavepacket, including its reflection and splitting at a potential barrier, can be seen in the time-dependent photoelectron energy distribution. This was nicely illustrated for the case of wavepacket motion on the $^1\Sigma_u^+$ double-minimum potential of Na_2 that arises from the avoided crossing of two diabatic states. Using the textbook example of electronic predissociation of the NaI molecule, these authors subsequently showed how pump–probe femtosecond photoelectron spectroscopy could also map nuclear wavepacket dynamics on two nonadiabatically coupled electronic states. While these early studies served to illustrate the utility and promise of pump–probe photoelectron spectroscopy for real-time mapping of wavepacket dynamics, they generally did not account for the dependence of the underlying photoionization amplitudes on geometry. Engel and coworkers, in fact, noted that the assumption of a position-independent transition dipole was questionable in cases where wavepackets moved through regions of avoided crossings and over rather large distances.[16] Furthermore, they stressed the importance of a robust description of the photoionization amplitudes for realistic predictions of pump–probe photoelectron spectra. It is also worth noting that the wavepacket studies of the femtosecond dynamics of NaI ionization and dissociative ionization by Charron and Suzor-Weiner,[17] which employed an empirical form to describe the covalent (NaI) to ionic (Na^+I^-) change of character in the transition dipole, yielded photoelectron and photoion spectra in encouraging agreement with recent measurements.[7]

In this paper we report on the results of detailed quantum-mechanical studies of energy- and angle-resolved femtosecond photoelectron spectra for wavepacket motion on the $^1\Sigma_u^+$ double-minimum state of Na_2 and on the potentials arising from the nonadiabatically coupled ionic (Na^+I^-) and covalent (NaI) states of NaI.[18] Both of these systems involve wavepacket motion through regions of an avoided crossing where the electronic character of the wavefunction changes dramatically with distance. In the case of Na_2 the avoided crossing of two diabatic states leads to an inner and an outer well with a barrier between them but wavepacket motion occurs on a single adiabatic potential. In the case of NaI the avoided crossing involves a covalent and an ionic state and wavepacket motion occurs on these two nonadiabatically coupled electronic states. The wavepacket dynamics in the NaI system can be expected to be extremely rich. In fact, the early experimental studies of NaI by Zewail and coworkers[1,19] were a watershed event that lead to an entirely new paradigm in the field of femtochemistry and established several new concepts for the dynamics of the chemical bond. Oscillatory motion of the wavepacket trapped within the adiabatic potential well formed from the avoided crossing was the first to demonstrate *resonance behavior*, in real time, of a bond converting from being covalent to being ionic in nature. Careful study of the angle- and time-resolved femtosecond photoelectron spectra of this system can be a useful window on the dynamics of this nonadiabatic coupling arising from electron transfer around the avoided crossing.

The results of these studies illustrate several important points. First, a robust description of the photoionization amplitudes and their dependence on geometry enhances the utility of femtosecond photoelectron spectroscopy as a probe of wavepacket dynamics and of the evolution of electronic structure. This is particularly true for wavepacket motion through an avoided crossing. In fact, in such regions, knowledge of the photoionization dynamics would seem essential in any unravelling of the wavepacket dynamics from the photoelectron signals. Secondly, as in the energy domain, photoelectron angular distributions convey richer structural and dynamical information than is contained in angle-averaged photoelectron spectra.[8,15] In fact, these angular distributions

not only provide insightful fingerprints of vibrational wavepacket dynamics, but their dependence on the relative polarizations of the pump and probe pulses can also be a useful real-time probe of molecular rotation.

Formulation

(a) Equations of motion for nuclear wavepackets

In the interest of brevity we choose to outline our formulation of femtosecond pump–probe energy- and angle-resolved photoelectron spectra in a form appropriate to ionization of wavepackets moving on a single adiabatic potential. This is the case for wavepackets on the double-minimum state of Na_2 where a potential barrier separates an inner and outer well. In a later section we will note certain key features and extensions that must be introduced to deal with the case of NaI where wavepacket motion occurs on nonadiabatically coupled surfaces.

Fig. 1 schematically illustrates the case of pump–probe photoelectron spectroscopy of vibrational wavepackets on the $^1\Sigma_u^+$ double-minimum state of Na_2 while Fig. 2 shows the relevant coordinate frames. A linearly polarized pulse of frequency ω_1 prepares a wavepacket on the excited state which is subsequently ionized by a time-delayed linearly polarized pulse of frequency ω_2. The molecule is oriented at angles (θ_R, ϕ_R) with respect to the polarization vector of the pump pulse and photoelectron angular distributions (θ_k, ϕ_k) are measured relative to the polarization of the probe. The angle between the probe and pump polarizations is θ_P and, without loss of generality, the probe is assumed to be in the xz plane of the pump frame. The interaction between the laser fields and the molecule is given by

$$\begin{aligned} V(t) &= V_1(t) + V_2(t) \\ &= E_{01} f_1(t)\sin(\omega_1 t)\vec{\varepsilon}_{\text{pump}} \cdot \vec{d} + \tfrac{1}{2}E_{02} f_2(t - \Delta T)\exp(-\omega_2(t - \Delta T))\vec{\varepsilon}_{\text{probe}} \cdot \vec{d}, \end{aligned} \tag{1}$$

where V_1 and V_2 represent the pump and probe fields respectively, E_{01} and E_{02} are field amplitudes $f_1(t)$ and $f_2(t - \Delta T)$ are Gaussian envelope functions, ΔT is the delay time between the two

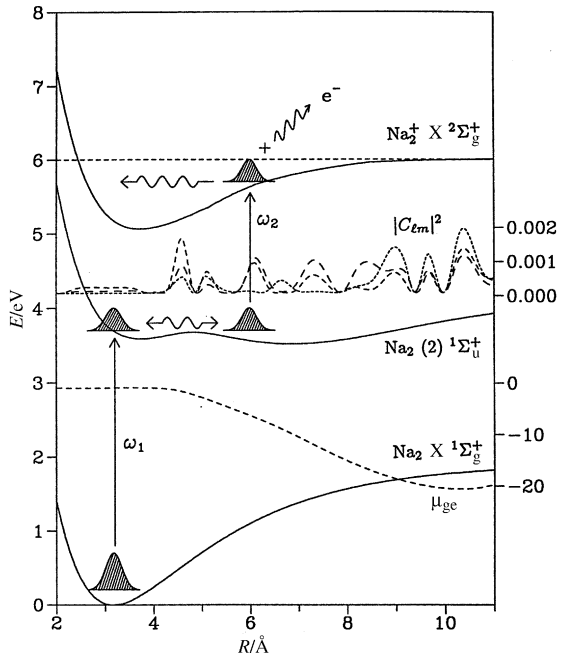

Fig. 1 Potential energy curves for the ground and double-minimum states of Na_2 and for the ground state of the ion. The photoionization coefficients (C_{lm}) for the molecule parallel to the pump and probe fields are shown for a kinetic energy of about 0.6 eV. The $l = 0$, 2 and 4 with $m = 0$ partial waves are denoted by long, medium and short dashed lines, respectively.

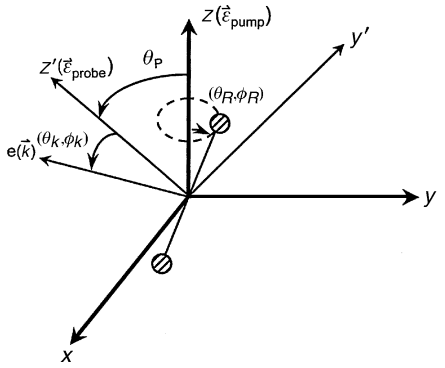

Fig. 2 Orientation of the molecule and pump and probe lasers: molecular orientation angles (θ_R, ϕ_R) are in the pump frame and photoelectron angles (θ_k, ϕ_k) in the probe frame.

pulses, $\vec{\varepsilon}_{\text{pump}}$ and $\vec{\varepsilon}_{\text{probe}}$ are the polarization vectors, and $\vec{d}$ is the electric dipole operator. We have also made the rotating wave approximation in V_2. The pump pulse produces a polarized distribution of molecules with a $\cos^2 \theta_R$ dependence with respect to $\vec{\varepsilon}_{\text{pump}}$.[20] Generally, the time scale for rotation ($\sim 10^{-10}$) is two to three orders of magnitude slower than that of vibrations ($\sim 10^{-13}$) and the probe laser with its pulse width of ~ 100 fs will probe this aligned distribution of slowly rotating molecules.

The Schrödinger equation can be written as

$$i\hbar \frac{\partial}{\partial t} \Psi(t) = [\hat{T}_N + \hat{H}_{el} + \hat{V}(t)]\Psi(t), \tag{2}$$

where $\hat{T}_N$ is the nuclear kinetic energy operator and $\hat{H}_{el}$ is the electronic Hamiltonian. The time-dependent wavefunction is expanded as

$$\Psi(\vec{r}, R, t) = \chi_g(R, t)\Phi_g(\vec{r}; R) + \chi_e(R, t)\Phi_e(\vec{r}; R) + \int d\vec{k}\chi_{\vec{k}}(R, t)\Phi_k^{(-)}(\vec{r}; R), \tag{3}$$

where Φ_g, Φ_e and $\Phi_k^{(-)}$ are eigenfunctions of $\hat{H}_{el}$ representing the ground, excited, and ionic states, respectively, $\vec{r}$ denotes electronic coordinates, and R the internuclear distance. Molecular rotation can be included in eqn. (3) by replacing R by $\vec{R}$. The functions χ_g, χ_e and $\chi_{\vec{k}}$ are wavepackets on the individual potential surfaces. Unlike excitation to a bound state, the final states in eqn. (3), $\chi_{\vec{k}}$, are characterized by photoelectron energies and angles, which eventually results in an infinitely many channelled problem. The electronic eigenfunctions satisfy the equations

$$\hat{H}_{el}\Phi_g(\vec{r}; R) = V_g(R)\Phi_g(\vec{r}; R) \tag{4}$$

$$\hat{H}_{el}\Phi_e(\vec{r}; R) = V_e(R)\Phi_e(\vec{r}; R) \tag{5}$$

and

$$\hat{H}_{el}\Phi_k^{(-)}(\vec{r}; R) = \left[V_{ion}(R) + \frac{(\hbar k)^2}{2m_e}\right]\Phi_k^{(-)}(\vec{r}; R), \tag{6}$$

where m_e is the electron mass and V_g, V_e and V_{ion} are the potential curves for the ground, excited, and ionic states. The $(-)$ sign on the continuum electronic wavefunction $\Phi_k^{(-)}$ indicates incoming-wave boundary conditions, canonically used to represent dissociation (ejection) in stationary-state scattering theory. These functions are a key ingredient of our studies of time-resolved photoelectron spectroscopy and obtaining them is challenging.

The equations of motion for the nuclear wavepackets are obtained as usual by projecting $\Phi_g(\vec{r}; R)$, $\Phi_e(\vec{r}; R)$, and $\Phi_k^{(-)}$ onto the Schrödinger equation and integrating over $\vec{r}$. This results in the

coupled equations

$$i\hbar \frac{\partial}{\partial t} \chi_g(R, t) = [\hat{T}_N + V_g(R)]\chi_g(R, t) + \langle \Phi_g(R) | V_1(t) | \Phi_e(R) \rangle \chi_e(R, t) \quad (7)$$

$$i\hbar \frac{\partial}{\partial t} \chi_e(R, t) = [\hat{T}_N + V_e(R)]\chi_e(R, t) + \langle \Phi_e(R) | V_1(t) | \Phi_g(R) \rangle \chi_g(R, t) + \int d\vec{k} \langle \Phi_e(R) | V_2(t; \Delta T) | \Phi_{\vec{k}}^{(-)}(R) \rangle \chi_{\vec{k}}(R, t) \quad (8)$$

and

$$i\hbar \frac{\partial}{\partial t} \chi_{\vec{k}}(R, t) = \left[\hat{T}_N + V_{ion}(R) + \frac{(\hbar k)^2}{2m_e} \right] \chi_{\vec{k}}(R, t) + \langle \Phi_{\vec{k}}^{(-)}(R) | V_2(t; \Delta T) | \Phi_e(R) \rangle \chi_e(R, t). \quad (9)$$

In deriving these equations we have assumed nonadiabatic behavior for the bound electronic wavefunctions and for the electronic continuum functions, *i.e.*,

$$\langle \Phi_g(R) | \hat{T}_N | \Phi_e(R) \rangle_{\vec{r}} \approx 0, \quad (10)$$

$$\int d\vec{k}' \langle \Phi_{\vec{k}}^{(-)} | \hat{T}_N | \Phi_{\vec{k}'}^{(-)} \rangle \simeq \int d\vec{k}' \langle \Phi_{\vec{k}'}^{(-)} | \Phi_{\vec{k}}^{(-)} \rangle \hat{T}_N | \chi_{\vec{k}'} \rangle = \hat{T}_N | \chi_{\vec{k}} \rangle. \quad (11)$$

Nonadiabatic coupling between the ground and excited states must be explicitly included for the NaI system. We will return to this in a later section and in future publications.[21,22]

To deal with the continuum part of $\Psi(\vec{r}, R, t)$ we expand $\Phi_{\vec{k}}^{(-)}$ and $\chi_{\vec{k}}$ in spherical harmonics, $Y_{lm}(\hat{k})$, about the polarization vector of the probe,

$$\Phi_{\vec{k}}^{(-)}(\vec{r}; R) = \sum_{lm} \Phi_{klm}^{(-)}(\vec{r}; R) Y_{lm}(\hat{k}), \quad (12)$$

$$\chi_{\vec{k}}(R, t) = \sum_{lm} \chi_{klm}(R, t) Y_{lm}(\hat{k}). \quad (13)$$

With these expressions the total wavefunction assumes the form

$$\Psi(\vec{r}, R) = \chi_g(R, t)\Phi_g(\vec{r}; R) + \chi_e(R, t)\Phi_e(\vec{r}; R) + \sum_{lm} \int dk\, k^2 (-1)^m \chi_{klm}(R, t) \Phi_{kl-m}^{(-)}(\vec{r}; R), \quad (14)$$

and eqns. (8) and (9) can be written as

$$i\hbar \frac{\partial}{\partial t} \chi_e(R, t) = [\hat{T}_N + V_e(R)]\chi_e(R, t) + \langle \Phi_e(R) | V_1(t) | \Phi_g(R) \rangle \chi_g(R, t) + \sum_{lm} \int k^2\, dk (-1)^m \langle \Phi_e(R) | V_2(t; \Delta T) | \Phi_{kl-m}^{(-)}(R) \rangle \chi_{klm}(R, t) \quad (15)$$

and

$$i\hbar \frac{\partial}{\partial t} \chi_{klm}(R, t) = \left[\hat{T}_N + V_{ion}(R) + \frac{(k\hbar)^2}{2m_e} \right] \chi_{klm}(R, t) + (-1)^m \langle \Phi_{kl-m}^{(-)}(R) | V_2(t; \Delta T) | \Phi_e(R) \rangle \chi_e(R, t). \quad (16)$$

The equations of motion for the wavepacket are now in the form of coupled equations specified by indices (g, e, k, l, m). The molecular applications of interest may require many ls which will result in hundreds of coupled equations.

(b) Dipole transition amplitudes

The dipole matrix element between the ground and excited states is given by

$$\langle \Phi_e | V_1(t) | \Phi_g \rangle = - E_{01} f_1(t) \sin(\omega_1 t) d_{eg} \cos(\theta_R) \tag{17}$$

with d_{eg} the magnitude of the dipole transition moment. Hence, under a sufficiently weak field, where Rabi oscillation is suppressed, the orientational distribution in the excited state is proportional to $\cos^2 \theta_R$. For Φ_e and Φ_g we employ high-level configuration-interaction wavefunctions obtained using electronic structure packages such as GAMESS or MOLPRO.

Determination of the matrix elements for photoionization of Φ_e is computationally challenging but essential to the objective of our studies. To obtain these matrix elements we use a frozen-core Hartree–Fock description of the final ionized state in which the wavefunction $\Phi_k^{(-)}$ is taken to be an antisymmetrized product of Hartree–Fock ion core orbitals, Φ_+, and a photoelectron orbital $\Phi_k^{(-)}$,

$$\Phi_k^{(-)} = \mathscr{A}(\Phi_+ \cdot \phi_k^{(-)}). \tag{18}$$

In this model the partial wave components, $\psi_{klm}^{(-)}$, of $\Phi_k^{(-)}$ satisfy a one-electron Schrödinger equation with the Hartree–Fock potential of the ion core, $V_{ion}(\vec{r}; R)$,

$$\left(-\frac{\hbar^2}{2m_e} \nabla^2 + V_{ion}(\vec{r}, R) - \frac{(\hbar k)^2}{2m_e} \right) \psi_{klm}^{(-)}(\vec{r}, R) = 0. \tag{19}$$

The Hartree–Fock model provides quite an adequate description of the wavefunctions and potentials of the ground ionic states of Na_2 and NaI over a wide range of internuclear distances. For example, they evolve to the correct dissociation limits. This is in stark contrast to the states of the neutral species where CI wavefunctions are necessary just to ensure the proper behavior at large internuclear distances. A robust description of the wavefunctions and potentials in regions of avoided crossings can require very extensive CI wavefunctions.

To proceed further we expand $\Phi_k^{(-)}$ in spherical harmonics, $Y_{lm}(\hat{k})$:

$$\Phi_k^{(-)} = \sum_{l,m,\lambda} \mathrm{i}^l \, \mathrm{e}^{-\mathrm{i}\eta_l} \mathscr{D}^l_{\lambda m}(\hat{R}') Y^*_{lm}(\hat{k}) \psi^{(-)}_{kl\lambda}(\vec{r}'; R), \tag{20}$$

where $\psi^{(-)}_{kl\lambda}$ is a partial-wave component of the photoelectron orbital in the molecular frame with momentum $\hbar\hat{k}$, λ is the projection of l in the molecular frame, $\vec{r}'$ is the electron coordinate in the molecular frame, $\mathscr{D}^l_{\lambda m}(\hat{R}')$ transforms the molecular-frame wavefunctions to those in the laboratory (probe) frame ($\psi^{(-)}_{klm}$ of eqn. (19)), and η_l is the Coulomb phase shift.[23] The dipole operator in the frame of the probe laser is given by

$$D_{\mu 0} = \sqrt{\frac{4\pi}{3}} \, r \sum_{\mu} \mathscr{D}^1_{\mu\mu_0}(\hat{R}'(Y_{1\mu}(\hat{r}'), \tag{21}$$

and hence the interaction between the probe laser and the molecule becomes

$$V_2 = \tfrac{1}{2} E_{02} f_2(t - \Delta T) \exp(-\mathrm{i}\omega_2(t - \Delta T)) \mathscr{D}_{\mu_0}. \tag{22}$$

The coupling matrix element between the excited state Φ^e and $\Phi_k^{(-)}$ can now be written as

$$\langle \Phi_k^{(-)}(R) | V_2(t - \Delta T) | \Phi_e(R) \rangle = \tfrac{1}{2} E_{02} f_2(t - \Delta T) \times \exp(-\mathrm{i}\omega_2(t - \Delta T)) \sum_{lm} C_{lm} Y_{lm}(\hat{k}), \tag{23}$$

where

$$C_{lm}(k, \theta_R, \phi_R, \theta_P) = \sqrt{\frac{4\pi}{3}} \sum_{\lambda\mu} I_{l\lambda\mu} \mathscr{D}^{l*}_{\lambda m}(\hat{R}') \mathscr{D}^1_{\mu\mu_0}(\hat{R}'), \tag{24}$$

and $I_{l\lambda\mu}$ is a partial-wave photoionization matrix element in the molecular frame. These are formed from dipole matrix elements between $|\Phi_+ \psi^{(-)}_{kl\lambda}\rangle$ and the components of the CI wavefunction used to describe Φ_e. For the case of ionization of an orbital ϕ_i into $\psi^{(-)}_{kl\lambda}$ these assume the

form

$$I^{(0)}_{l\lambda\mu}(R) = (-\mathrm{i})^l\, \mathrm{e}^{\mathrm{i}\eta_l} \sum_{l_0\lambda_0} \langle \psi^{(-)}_{kl\lambda} \,|\, r Y_{1\mu}(\hat{r}') \,|\, \phi_{\mathrm{i},\, l_0\lambda_0}(r) Y_{l_0\lambda_0}(\hat{r}') \rangle. \tag{25}$$

The C_{lm} coefficients contain the dynamical information needed to describe the photoionization of an oriented Na_2 or NaI molecule. The partial-wave components of the photoelectron orbital, $\psi^{(-)}_{kl\lambda}$, are obtained numerically using a procedure outlined in detail elsewhere.[23] The angular momentum coupling in molecular photoelectrons arising from torques exerted by the ion core can be seen in the single-center expansion of $\psi^{(-)}_{kl\lambda}$ for a linear molecule

$$\psi^{(-)}_{kl\lambda}(\vec{r};\, R) = \sum_{l'} g_{ll'\lambda}(r,\, R) Y_{l'\lambda}, \tag{26}$$

where $g_{ll'\lambda}(r, R)$ is a radial component of the partial-wave function $\psi^{(-)}_{kl\lambda}(\vec{r};\, R)$. Use of photoelectron orbitals which correctly incorporate such angular momentum coupling is essential for a quantitative description of molecular photoionization.

(c) Coupled equations

Insertion of eqns. (17) and (23) into eqns. (15) and (16) yields the following equations of motion for the nuclear wavepackets

$$\mathrm{i}\hbar \frac{\partial}{\partial t} \chi_{\mathrm{g}}(R,\, t) = [\hat{T}_{\mathrm{N}} + V_{\mathrm{g}}]\chi_{\mathrm{g}}(R,\, t) + V_{\mathrm{ge}}\, \chi_{\mathrm{e}}(R,\, t), \tag{27}$$

$$\mathrm{i}\hbar \frac{\partial}{\partial t} \chi_{\mathrm{e}}(R,\, t) = [\hat{T}_{\mathrm{N}} + V_{\mathrm{e}}]\chi_{\mathrm{e}}(R,\, t) + V_{\mathrm{eg}}\, \chi_{\mathrm{g}}(R,\, t) + \frac{1}{2} \sum_{lm} \int \mathrm{d}k\; k^2 E_{02}\, f_2(t - \Delta T) \times \exp(\mathrm{i}\omega_2(t - \Delta T)) C^*_{lm}(k,\, \theta_R,\, \phi_R,\, \theta_{\mathrm{P}}) \chi_{klm}(R,\, t), \tag{28}$$

and

$$\mathrm{i}\hbar \frac{\partial}{\partial t} \chi_{klm}(R,\, t) = \left[\hat{T}_{\mathrm{N}} + V_{\mathrm{ion}} + \frac{(\hbar k)^2}{2m_{\mathrm{e}}} \right] \chi_{klm}(R,\, t) + \tfrac{1}{2} E_{02}\, f_2(t - \Delta T) \exp(-\mathrm{i}\omega_2(t - \Delta T)) C_{lm}(k,\, \theta_R,\, \phi_R,\, \theta_{\mathrm{P}}) \chi_{\mathrm{e}}(R,\, t). \tag{29}$$

In eqns. (26) and (27), $V_{\mathrm{eg}} = \langle \Phi_{\mathrm{e}} \,|\, V_1(t) \,|\, \Phi_{\mathrm{g}} \rangle$ and V_{ge} its complex conjugate.

Discretization of the continuum integration in eqn. (27) *via* a finite quadrature such as a Gauss–Legendre quadrature leads to

$$\mathrm{i}\hbar \frac{\partial}{\partial t} \chi_{\mathrm{e}}(R,\, t) = [\hat{T}_{\mathrm{N}} + V_{\mathrm{e}}]\chi_{\mathrm{e}}(R,\, t) + V_{\mathrm{eg}}\, \chi_{\mathrm{g}}(R,\, t) + \frac{1}{2} \sum_{j=1}^{N_k} \sum_{lm} E_{02}\, k_j^2 \omega_j\, f_2(t - \Delta T) \times \exp(\mathrm{i}\omega_2(t - \Delta T)) C^*_{lm}(k_j,\, \theta_R,\, \phi_R,\, \theta_{\mathrm{P}}) \chi_{kjlm}(R,\, t), \tag{30}$$

where N_k is the number of quadrature points and ω_j are the weights. This discretization leads to a finite set of coupled equations of motion. These time-dependent coupled equations are solved using the split-operator technique.[24,25] Details of the quadrature employed and several methodological issues associated with these coupled equations and their solutions are discussed in ref. 21 and 22. The present applications to Na_2 and NaI result in several hundred coupled equations.

Applications

(a) The double-minimum state of Na_2

Fig. 1 shows the potential energy curves for the ground and double-minimum Σ_{u}^+ states of Na_2 and the ground state of the ion. This double-minimum state has been studied extensively[26] and results from an avoided crossing of two diabatic states; the first of these is a Rydberg state and the second has substantial ionic character in the outer well. Details of the wavefunctions and potential curves employed in these studies are given in ref. 22.

The C_{lm} coefficients can be expected to reflect the evolution of the photoionization dynamics with internuclear distance in this state with its avoided crossing and increasing ionic character in

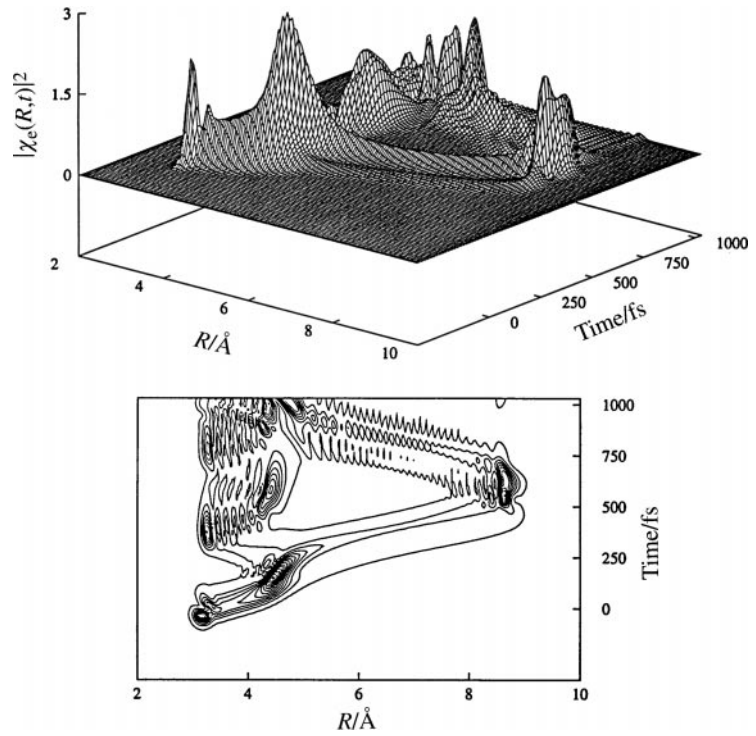

Fig. 3 Perspective view and contour plot of the wavepackets, $|\chi_e(R, t)|^2$, for a pump pulse photon of 3.6763 eV.

the outer well. These coefficients for the case of polarization vectors of the pump and probe pulses parallel to the molecular axis and for a photoelectron energy of about 0.6 eV are shown as a function of internuclear distance in Fig. 1. For this state of Na_2 only even *l*s arise, while for this parallel arrangement only $m = 0$ terms are allowed. These C_{lm}s display several important features. Among these, we note the striking change in the C_{lm}s in the barrier region where the avoided crossing occurs. Furthermore, the large magnitude of the C_{lm}s around the barrier should exert an influence on the ion signal as the wavepacket moves through this region. In the barrier region the $l = 2$ component of C_{lm} is dominant. These C_{lm}s oscillate across the well and at large distances where the state acquires significant ionic character, the $l = 4$ component of C_{lm} is the largest.

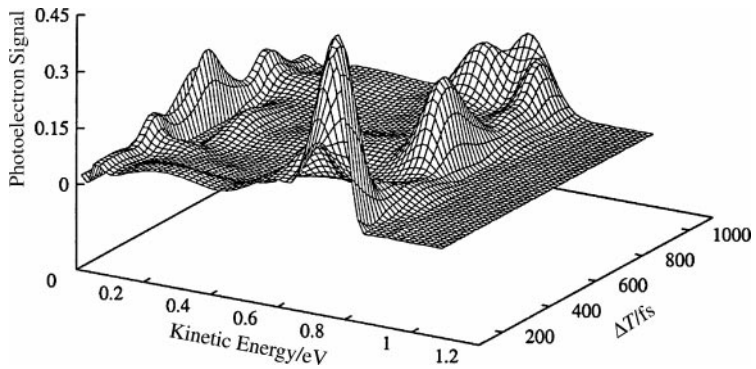

Fig. 4 Photoelectron signal *vs.* kinetic energy and delay-time. The pump photon energy is 3.6763 eV and puts the wavepacket at the barrier. Pump and probe polarizations are parallel.

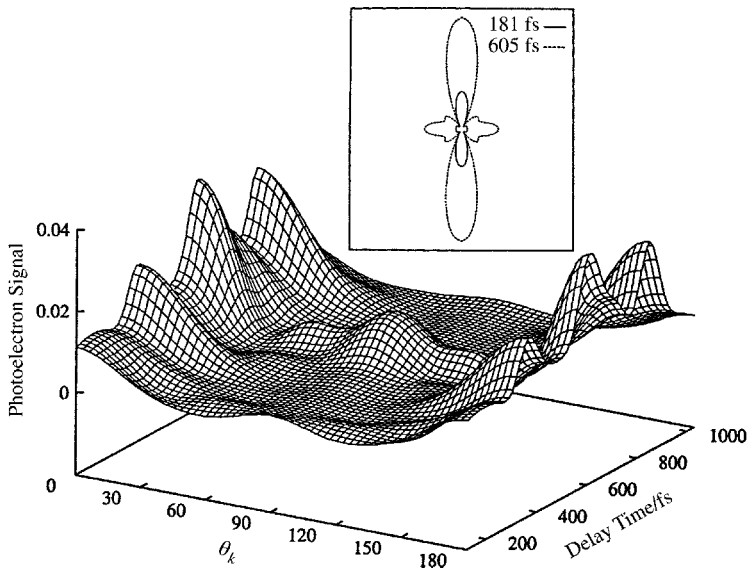

Fig. 5 Photoelectron angular distributions for various delay times and a photoelectron energy of 0.0224 eV.

We now look at a few features of the pump–probe photoelectron spectra for wavepacket motion on this state and explore how they may reflect the underlying photoionization dynamics. Our procedures for extracting energy- and angle-resolved photoelectron spectra from the χ_{klm} of eqns. (28) and (29) are outlined in ref. 22. We have previously shown that for wavepacket motion in the inner well (pump photon energy of 3.62 eV), the near-vanishing values of the C_{lm}s for all (k_j, l, m) in a narrow range to the left of the potential barrier result in a very low photoelectron signal whenever the wavepacket hits this region and hence in an oscillatory ion signal as a function of delay time.[22] We now examine some additional features but for a wavepacket formed by a pump pulse with an energy on the top of the potential barrier. For this case the pump photon energy is 3.6763 eV. Fig. 3 shows the behavior of such a wavepacket formed by a pulse with a FWHM of 120 fs and centered at $t = 0$. It takes the wavepacket about 100 fs to reach the barrier at 4.7 Å where it splits into two components: a lower energy component that is reflected into the inner well and reaches its inner turning point at $t = 400$ and 800 fs and a higher energy component in the outer well that reaches its outer turning point at 600 fs and rejoins the inner well component at $t = 1000$ fs.

The photoelectron energy distributions for different delay times for ionization of this wavepacket by a probe photon of 2.28 eV and with the pump and probe polarizations parallel are shown in Fig. 4. The probe pulse has a FWHM of 40 fs. The strong peak around 0.7 eV occurs as the wavepacket moves slowly through the barrier where the photoionization amplitudes are large (Fig. 1). A strong peak at low photoelectron energy is seen around $\Delta T = 600$ fs when the wavepacket reaches its outer turning point where only low kinetic energy photoelectrons can be ejected since almost all the energy goes into potential energy of Na_2^+.

It is instructive to look at the photoelectron angular distributions for these spectra to see how they may reflect photoionization dynamics. Fig. 5 shows these distributions for various delay times for a photoelectron energy of 0.0224 eV. The distribution for a delay time of 600 fs is particularly interesting. This feature arises from the motion of the wavepacket around the outer turning point where the C_{lm} for $l = 4$ is quite strong. Even at this photoelectron energy the dominance of such a high partial wave is very evident in these distributions. The much weaker signal at this energy for a delay time of 181 fs comes from the barrier region and, as indicated by the C_{lm} values, shows d character.

Fig. 6 shows photoelectron angular distributions for the probe pulse (2.28 eV) polarized parallel and perpendicular to the pump pulse (3.68 eV) for a kinetic energy of 0.5967 eV. These angular

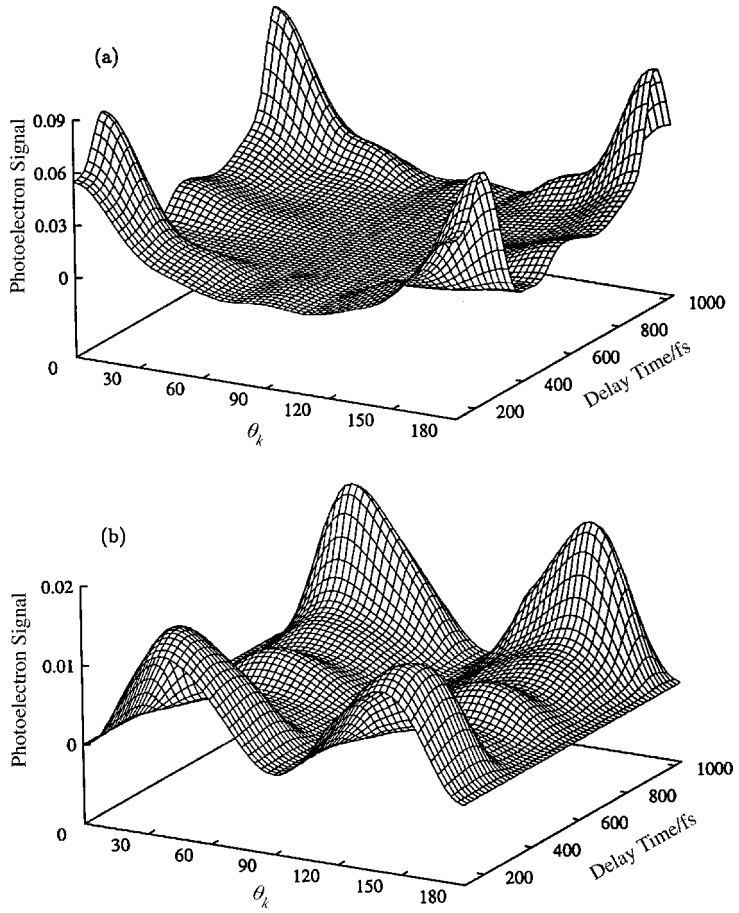

Fig. 6 Photoelectron angular distributions for different delay times for (a) parallel and (b) perpendicular polarizations of the pump and probe pulses. The photoelectron energy is about 0.6 eV. See text.

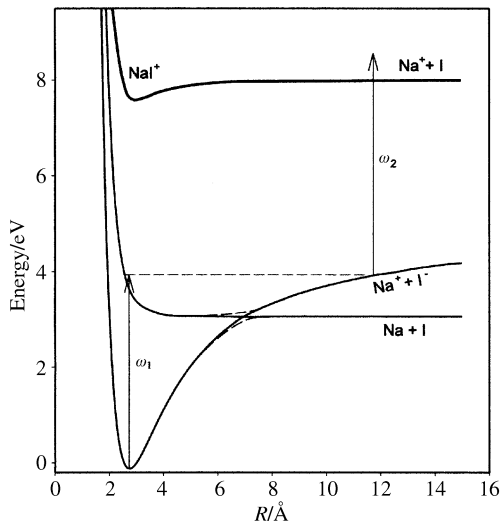

Fig. 7 Illustration of the adiabatic and diabatic potentials and pump–probe scheme for NaI.

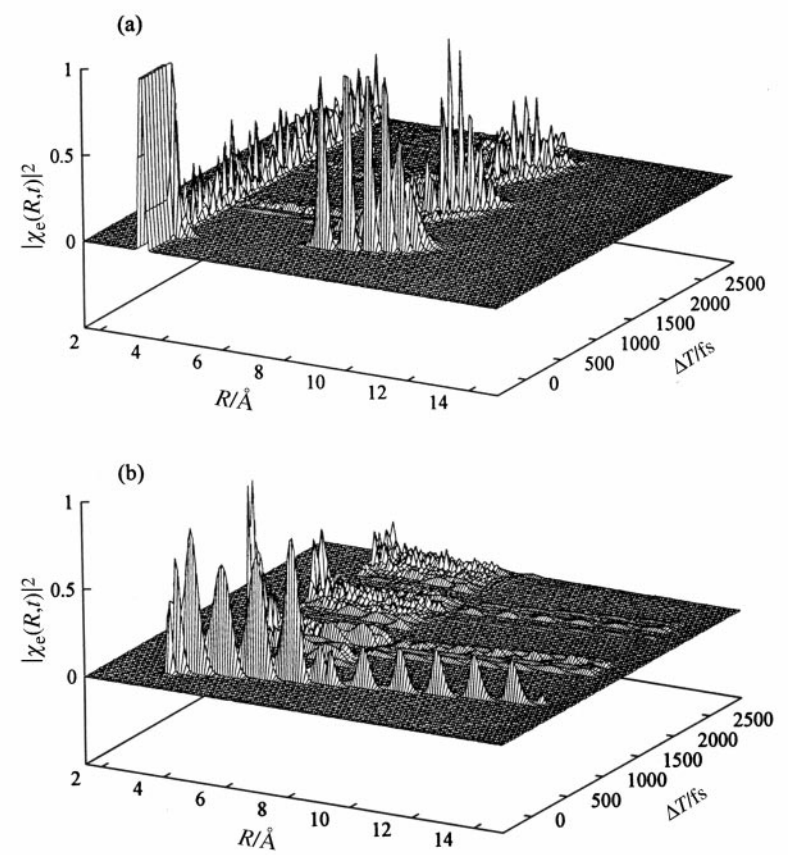

Fig. 8 Wavepacket motion ($|\chi_e(R, t)|^2$) (a) on the V_1 (ionic) diabatic potential of NaI and (b) on the V_2 (covalent) diabatic potential. The pump photon energy is 3.5 eV.

distributions are strikingly different for the two cases. For the parallel case the angular distributions are clearly of the d_{z^2} type while they show d_{yz} behavior for the perpendicular case. This behavior is consistent with symmetry considerations for the dipole interaction. Such dependence of photoelectron angular distributions on the orientation of the probe and molecular axis can be of value for monitoring molecular rotation.

(b) NaI

Extensive studies by Zewail and coworkers have established NaI as a benchmark system for monitoring wavepacket evolution in the time domain.[1,2,19] In these experiments a femtosecond pump laser pulse prepares a wavepacket on the lowest lying covalent excited state which is coupled nonadiabatically to the ground state of the molecule (Fig. 7). The wavepacket oscillates across the adiabatic potential well formed by the avoided crossing of a covalent (NaI) diabatic state and an ionic (Na^+I^-) diabatic state. With this oscillatory motion the bound converts from being covalent to being ionic in the region of the avoided crossing. In these studies the time-evolution of the wavepacket was monitored by excitation to a higher electronic state and fluorescence from this state at different delay times.[19] More recently Jouvet *et al.* have followed the wavepacket evolution on this A excited state of NaI by time-resolved detection of photoelectrons and photoions.[7] The measured photoelectron spectra and molecular and atomic ion kinetic energy distributions of these studies provide an insightful characterization of the nuclear dynamics of this system. Several theoretical studies of the pump–probe photoelectron kinetic energy distributions[16,17] and of dissociative ionization[17] of this NaI system have also been reported.

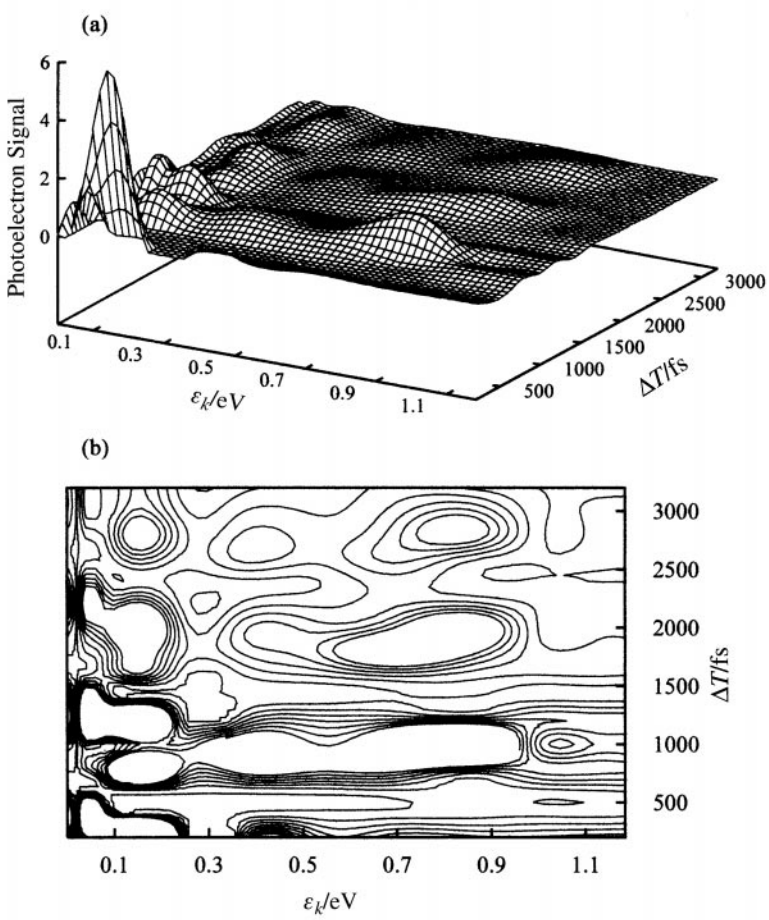

Fig. 9 Photoelectron signal *vs.* kinetic energy and delay time for ionization of wavepackets on the covalent and ionic potentials of NaI by a probe pulse of 5 eV and FWHM of 100 fs. The pump and probe polarizations are parallel: (a) perspective plot and (b) contour. See text.

The femtosecond pump–probe photoelectron spectra of this wavepacket with its oscillatory motion between a covalent and an ionic potential with its associated leakage of free atoms onto the covalent surface can be expected to have significant dynamical content. The energy- and angle-resolved photoelectron spectra should surely reflect the large difference in the photoionization amplitudes between the ionic and covalent surfaces. For example, the photodetachment cross section of I^- ($Na^+ + I^-$) is two orders of magnitude larger than the cross section for photoionization of Na (Na + I).[27] Here we report some preliminary results of detailed quantum-mechanical studies of wavepacket motion on these coupled covalent and ionic states of NaI. One of the main objectives of these studies is to explore the potential of angle-resolved pump–probe photoelectron spectra for probing the real-time dynamics of the intramolecular electron transfer occuring in the region of the nonadiabatic transition between the covalent and ionic states ($NaI \rightarrow Na^+ + I^-$). In such studies it would seem essential to employ robust descriptions of the potential surfaces and of the geometry- and energy-dependent photoionization amplitudes.

These applications require several important extensions of our formulation of pump–probe energy- and angle-resolved photoelectron spectra outlined in a previous section of this paper. The most important of these is to provide for nonadiabatic coupling between the ionic and covalent states. In these studies we employ diabatic potential surfaces, obtained from accurate adiabatic surfaces, by a procedure that provides the coupling elements between these diabatic surfaces and the transformation matrix between the diabatic and adiabatic representations. The inverse of this

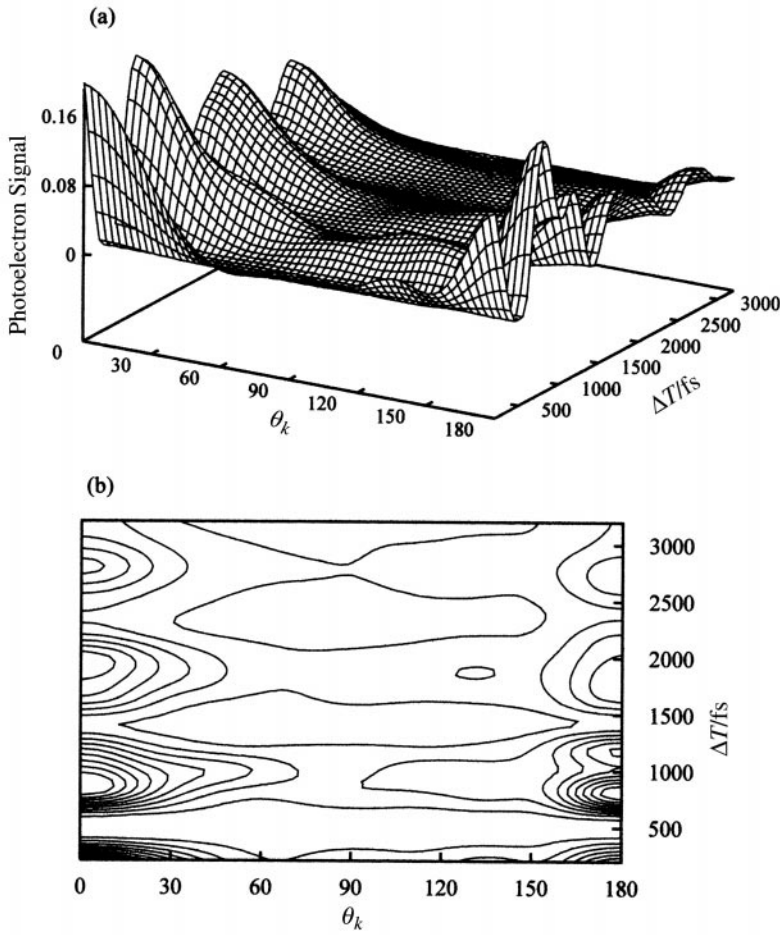

Fig. 10 Photoelectron angular distributions integrated over kinetic energies for ionization of the wavepackets on the covalent and ionic states of NaI by a probe pulse of 5 eV. The pump and probe polarizations are parallel to the molecular axis.

transformation is used in transforming dipole transition amplitudes from the adiabatic to diabatic representation. Details of this procedure will be presented elsewhere.[21]

While calculations employing very high-level adiabatic potential surfaces obtained with the MOLPRO electronic structure code are underway, we report results using surfaces of slightly lower quality which, for example, did not incorporate spin–orbit contributions to the energy. We have since found that it is essential to include spin–orbit interactions in order to obtain the shape of the excited state potential around the minimum of the ground state. These lower-quality surfaces have been shifted slightly to ensure that essential features such as the crossing point are realistically represented.

Fig. 8 shows the wavepackets on these ionic (V_1, lower) and covalent (V_2, upper) states for a linearly polarized pump pulse of 3.5 eV with a FWHM of 100 fs and centered at $t = 0$. The use of diabatic potentials provides a very pictorial view of the wavepacket motion. The wavepacket reaches the crossing point between V_1 and V_2 and undergoes bifurcation there. The component of the wavepacket that continues along V_2 (covalent) represents dissociation into neutral atoms. The component on the ionic surface (V_1) reaches its righthand turning point near 11 Å at around 600 fs. This component returns to the crossing point at around 750 fs, bifurcates again with its component on V_2 (covalent) reaching the lefthand turning point at around 1 ps.

For ionization of these wavepackets we choose a probe pulse with a photon energy of 5 eV which is just sufficient to ionize the wavepacket on V_2 (covalent) beyond the crossing point. This pulse has a FWHM of 100 fs and its polarization is parallel to that of the pump pulse. Fig. 9 shows the resulting photoelectron energy distributions as a function of delay time ΔT. The peaks in this spectrum help in mapping the wavepacket motion and provide valuable insight. For example, the prominent peaks at almost zero kinetic energy seen at 300–500 fs, 1000–1500 fs, 1800–2400 fs and 2800–3300 fs arise from ionization of the wavepackets on the V_2 diabatic curve after passing the crossing point to the neutral dissociation channel. These peaks become lower, broader, and less structured as the delay time increases. This decrease in peak heights reflects the decreasing population due to leakage through the crossing point, while the less structured shape of these features reflects the increasing complexity of the wavepacket in the molecular region. Peaks of slightly lower intensity and at a slightly higher energy stem from packets moving up on the V_1 surface shortly after passing through the crossing point. The rather low peaks around 0.8 eV and 1000 fs come from the wavepacket on the inner region of the V_2 diabatic potential. These high energy photoelectrons must arise from ionization of the wavepacket near the minimum of the ion potential curve. These regions of high photoelectron energy obviously favor formation of the molecular ion. Dissociative ionization should occur in regions of low photoelectron energy and hence large nuclear kinetic energy.

Fig. 10 shows the photoelectron angular distributions of these spectra integrated over all kinetic energies for ionization of the wavepackets on these surfaces (Fig. 8). These angular distributions provide insight into the dynamics of photoelectron ejection as the wavepacket passes through the avoided crossing on its way from the NaI surface to the Na^+I^- surface. The iodine atom is at $\theta = 180°$ while sodium is at $\theta = 0°$. A typical situation of interest can be seen in the series of peaks at $\Delta T = 800$ fs, $\theta = 180°$ (I-side), $\Delta T = 1000$ fs, $\theta = 0°$ (Na-side) and $\Delta T = 1200$ fs, $\theta = 180°$ (I-side). The first of these peaks arises from wavepacket motion on V_1 (ionic) beyond the crossing point, the second peak comes from the wavepacket moving into the inner region of V_2 (neutral), and the third peak arises from wavepacket components that have come back to the outer region of V_1 (ionic). This indicates that electron ejection is from the Na-side when a wavepacket is in the inner region (covalent) while photoelectrons are launched from the iodine side when a packet is on the ionic curve, *i.e.*, the direction of photoelectron ejection changes dramatically as the packet passes through the crossing point.

These preliminary results of our studies of angle- and energy-resolved pump–probe photoelectron spectra of NaI suggest that such spectra can be a useful window on the real-time dynamics of electron transfer in NaI and perhaps in a few other small and well-chosen systems. Angle-resolved spectra would appear to be particularly valuable in such studies. Straightforward extensions of these studies of the pump–probe photoelectron spectra of NaI are under way. We are examining these spectra at different molecular orientations, for different orientations of the pulse polarization and the molecular axis, and with chirped pulses. We are also exploring the sensitivity of these spectra on features on the potential surfaces.

Concluding remarks

The results of these studies serve to illustrate how a quantitative understanding of the molecular photoionization amplitudes and their dependence on geometry can enhance the utility of time-resolved femtosecond photoelectron spectra as a probe of wavepacket dynamics and of the evolution of electronic structure. This is particularly so for wavepacket motion through avoided crossings where these amplitudes can evolve rapidly. The crossing region between the covalent and ionic states of NaI provides an excellent example of this. Furthermore, as in energy-resolved photoelectron spectroscopy, angular distributions of pump–probe spectra can convey rich dynamical information not seen in angle-integrated photoelectron spectra. In fact, the angular distributions in the crossing region of the ionic and covalent NaI states of these studies suggest that angle-resolved pump–probe photoelectron spectra may be a useful probe of the real-time dynamics of intramolecular electron transfer. Such spectra may provide useful snapshots of the motion in these nonadiabatic transitions due to electron transfer. Studies addressing these and related issues are under way. Because such studies must rely on a robust description of photoionization amplitudes, applications to small polyatomic systems should be most rewarding.

Acknowledgement

This work was supported by a grant from the Ministry of Education, Science and Culture (Japan) and the National Science Foundation (USA).

References

1 T. S. Rose, M. J. Rosker and A. H. Zewail, *J. Chem. Phys.*, 1988, **88**, 6672.
2 A. H. Zewail, *Femtochemistry: Ultrafast Dynamics of the Chemical Bond*, World Scientific, Singapore, vol. 1 and 2.
3 *Femtochemistry*, ed. J. Manz and L. Wöste, Wiley-VCH, Weinheim, 1995.
4 *Chemical Reactions and Their Control on the Femtosecond Time Scale*, *Adv. Chem. Phys.*, 1997, **101**, ed. P. Gaspard, I. Burghard, I. Prigogine and S. A. Rice, Wiley, New York.
5 (*a*) I. Fischer, D. M. Villeneuve, M. J. J. Vrakking and A. Stolow, *J. Chem. Phys.*, 1995, **102**, 5566; (*b*) V. Blanchet, M. Z. Zgierski, T. Seideman and A. Stolow, *Nature*, 1999, **401**, 52.
6 A. Assion, M. Geisler, J. Helbing, V. Seyfried and T. Baumert, *Phys. Rev. A*, 1996, **54**, R4605.
7 C. Jouvet, S. Martrenchard, D. Solgadi, C. Dedonder-Lardeux, M. Mons, G. Grégoire, I. Dimicoli, F. Piuzzi, J. P. Visticot, J. M. Mestdagh, P. D'Oliveira, P. Meynadier and M. Perdrix, *J. Phys. Chem.*, 1997, **101**, 2555.
8 J. A. Davies, J. E. LeClaire, R. E. Continetti and C. C. Hayden, *J. Chem. Phys.*, 1999, **111**, 1.
9 T. Baumert, J. L. Herek and A. H. Zewail, *J. Chem. Phys.*, 1993, **99**, 4430.
10 T. Baumert and G. Gerber, *Adv. At. Mol. Opt. Phys.*, 1995, **35**, 163.
11 H. Ruppe, S. Rutz, E. Schneiber and L. Wöste, *Chem. Phys. Lett.*, 1996, **257**, 356.
12 X. Song, C. W. Wilkerson, J. Lucio, S. Pauls and J. P. Reilly, *Chem. Phys. Lett.*, 1990, **174**, 377.
13 M. R. Dobber, W. J. Buma and C. A. de Lange, *J. Chem. Phys.*, 1993, **99**, 836.
14 J. A. Syage, *Z. Phys. D*, 1994, **30**, 1.
15 T. Suzuki, L. Wang and K. Kohguchi, *J. Chem. Phys.*, 1999, **111**, 4859.
16 For example, V. Engel, *Chem. Phys. Lett.*, 1991, **178**, 130; Ch. Meier and V. Engel, *Chem. Phys. Lett.*, 1993, **212**, 691; M. Braun, Ch. Meier and V. Engel, *J. Chem. Phys.*, 1996, **105**, 530.
17 E. Charron and A. Suzor-Weiner, *J. Chem. Phys.*, 1998, **108**, 3922.
18 R. S. Berry, *J. Chem. Phys.*, 1957, **27**, 1288.
19 For example, P. Cong, G. Roberts, J. L. Herek, A. Mohktari and A. H. Zewail, *J. Phys. Chem.*, 1996, **100**, 7832.
20 For example, M. Gruebele and A. Zewail, *J. Chem. Phys.*, 1993, **98**, 883.
21 Y. Arasaki, K. Takatsuka, K. Wang and V. McKoy, manuscript in preparation.
22 Y. Arasaki, K. Takatsuka, K. Wang and V. McKoy, *J. Chem. Phys.*, 2000, **112**, 8871.
23 (*a*) R. R. Lucchese, D. K. Watson and V. McKoy, *Phys. Rev. A*, 1982, **25**, 2572; (*b*) R. R. Lucchese, K. Takatsuka and V. McKoy, *Phys. Rep.*, 1986, **131**, 147.
24 (*a*) D. Kosloff and R. Kosloff, *J. Comput. Phys.*, 1983, **52**, 35; (*b*) R. Kosloff, *J. Phys. Chem.*, 1988, **92**, 2087.
25 K. Takahashi and K. Ikeda, *J. Chem. Phys.*, 1993, **99**, 8680.
26 D. L. Cooper, R. F. Barrow, J. Verges, C. Effantin and J. D. Incan, *Can. J. Phys.*, 1984, **62**, 1543.
27 (*a*) R. D. Hudson and V. L. Carter, *J. Opt. Soc. Am.*, 1967, **95**, 578; (*b*) V. Radojevic, H. P. Kelly and W. R. Johnson, *Phys. Rev. A*, 1987, **35**, 2117.